

# Temporal Overlapping Prediction: A Self-supervised Pre-training Method for LiDAR Moving Object Segmentation

Ziliang Miao<sup>1</sup> Runjian Chen<sup>1\*</sup> Yixi Cai<sup>2</sup> Buwei He<sup>2</sup>  
Wenquan Zhao<sup>3</sup> Wenqi Shao<sup>4</sup> Bo Zhang<sup>4</sup> Fu Zhang<sup>1†</sup>

<sup>1</sup>The University of Hong Kong <sup>2</sup>KTH Royal Institute of Technology  
<sup>3</sup>Southern University of Science and Technology <sup>4</sup>Shanghai AI Laboratory

{miaozi, rjchen}@connect.hku.hk {yixica, buwei}@kth.se  
zhaowq2021@sustech.edu.cn {shaowenqi, zhangbo}@pjlab.org.cn fuzhang@hku.hk

## Abstract

Moving object segmentation (MOS) on LiDAR point clouds is crucial for autonomous systems like self-driving vehicles. Previous supervised approaches rely heavily on costly manual annotations, while LiDAR sequences naturally capture temporal motion cues that can be leveraged for self-supervised learning. In this paper, we propose **Temporal Overlapping Prediction (TOP)**, a self-supervised pre-training method that alleviate the labeling burden for MOS. **TOP** explores the temporal overlapping points that commonly observed by current and adjacent scans, and learns spatiotemporal representations by predicting the occupancy states of temporal overlapping points. Moreover, we utilize current occupancy reconstruction as an auxiliary pre-training objective, which enhances the current structural awareness of the model. We conduct extensive experiments and observe that the conventional metric Intersection-over-Union (IoU) shows strong bias to objects with more scanned points, which might neglect small or distant objects. To compensate for this bias, we introduce an additional metric called  $mIoU_{obj}$  to evaluate object-level performance. Experiments on nuScenes and SemanticKITTI show that **TOP** outperforms both supervised training-from-scratch baseline and other self-supervised pre-training baselines by up to 28.77% relative improvement, demonstrating strong transferability across LiDAR setups and generalization to other tasks. Code and pre-trained models will be publicly available upon publication.

## 1. Introduction

Moving Object Segmentation (MOS) on LiDAR data aims to segment moving points from the entire LiDAR scan and provides autonomous systems [9, 33, 34, 50, 54] with important clues in localization and dynamic obstacle avoidance, which enables better planning of collision-free trajectories in dynamic scenes. However, per-point manual labeling of moving objects [3, 6, 9] is both costly and labor-intensive. Meanwhile, self-supervised pre-training achieves significant success in Natural Language Processing (NLP) [5, 13, 19, 30, 40], Computer Vision (CV) [14, 17, 18, 41, 51], and 3D Vision [39, 55, 58, 59], enabling the learning of transferable embeddings from unlabeled raw data. This motivates us to pre-train a backbone using raw LiDAR data in a self-supervised manner and then fine-tune it for MOS, which has limited expensive labeled data.

The MOS task heavily relies on temporal information, including the positions of an object at different times and the changing relative positions of an object to its surroundings. In the literature involving temporal information of LiDAR data, an intuitive approach is to utilize LiDAR observation forecasting as a self-supervised pre-training method for MOS. The forecasting task includes point cloud forecasting [23, 32, 52, 53, 60] and occupancy forecasting [1], which focus on predicting future scans or occupancy maps based on past and current LiDAR scans and poses. However, utilizing forecasting as a pre-training method for MOS presents certain limitations: (1) The forecasting task is more complex and advanced than MOS. Forecasting a static object mainly requires geometric information to reconstruct the unseen parts of the object from a novel sensor view. For moving objects, beyond geometry, it is essential to extract temporal features such as the object’s kinematics and interactions between objects and their surroundings. Hence, relying on forecasting as a pre-training step for MOS could

\*Project lead.

†Corresponding author.

be overly demanding. (2) Existing methods [1, 23] inevitably learn a “flow” when using raw future observations as supervision. This complex “flow” information represents the relationship between past observations’ embeddings and future observations. Current approaches either implicitly learn this flow through simple feature broadcasting [23] or explicitly predict it [1], lacking direct supervision similar to the scene flow task [29, 61, 62]. Thus, the learned “flow” tends to be noisy. Relying on this noisy “flow” for deterministic future observation predictions (as opposed to the generative approach [60]) can lead to network overfitting, thereby reducing its transferability to target downstream tasks.

To overcome these two limitations and incorporate temporal information for MOS self-supervised pre-training, we propose **Temporal Overlapping Prediction**. **TOP** explores the temporal occupancy states of temporal overlapping points observed by both the current scan and adjacent past or future scans for pre-training. The rationale for this lies in the potential for moving objects to cause the current occupancy states of temporal overlapping points to differ from the states at other observed times, as illustrated in Figure 1. We first pre-process the spatial positions and temporal occupancy states of the overlapping points with beam divergence [31], which is a physical characteristic of LiDAR. This LiDAR nature helps avoid discretization errors caused by manually setting a fixed voxel resolution. Then, we pre-train the encoder by predicting the pre-processed temporal occupancy states, which simplifies the task compared to directly forecasting LiDAR observations. Based on a distinct temporal correlation between LiDAR beams at different times established by the pre-processing, our pre-training factors out either implicit or explicit learning of a noisy “flow”. Additionally, since understanding current states is also important for MOS, we add a reconstruction term for optimization.

We assess the MOS performance on the nuScenes [6] and SemanticKITTI [3] datasets. Previous evaluations of nuScenes MOS in [34, 46] directly convert object attributes to MOS labels. However, these attributes do not precisely reflect the motion state of the object, and not all objects have attributes. Thus, we combine object attributes with object speed calculated based on bounding boxes to obtain refined nuScenes MOS labels. In the experiments, we observe that the conventional metric Intersection-over-Union (IoU) for MOS exhibits a significant bias towards objects that have a larger number of scanned points, potentially overlooking smaller or more distant objects. Thus, we propose an additional object-level evaluation metric  $mIoU_{obj}$  to take these objects into account.

We conducted few-shot fine-tuning experiments on the nuScenes dataset with different amounts of labeled data. Results show that **TOP** achieves improvements over the supervised training-from-scratch baseline [33] and outper-

forms other self-supervised pre-training baselines, such as state-of-the-art (SOTA) LiDAR observation forecasting methods [1, 23] and the occupancy-based 3D pre-training method [4]. The results of our few-shot cross-dataset experiments on the SemanticKITTI dataset further highlight the superior transferability of **TOP** pre-training compared to various baselines. Additionally, we fine-tune the pre-trained backbone on the nuScenes semantic segmentation task in a few-shot setting, demonstrating the potential generalization capability of **TOP** across more tasks.

## 2. Related Works

**Moving Object Segmentation.** Existing supervised MOS methods can be grouped into projection-based and voxel-based approaches. The early MOS methods [9, 11, 24, 45] project 3D LiDAR data to range images and embed the range residual images by 2D backbone. These methods suffer from imprecise boundaries when re-projecting 2D outputs to 3D point clouds [34]. Recent methods [33, 34, 46, 50] utilize the sparse convolution backbone to directly embed voxelized point clouds. 4DMOS [33] first employs sparse 4D UNet [12] and makes it the SOTA backbone for MOS. For unsupervised approaches, several scene flow methods [2, 16, 44, 48] decouple the per-point flow to an ego-motion flow for static points and a non-rigid flow for moving points, which provides a byproduct of MOS [33]. However, these approaches using only two adjacent scans, encounter challenges in identifying slowly moving objects [33]. MOTS [25] proposes a label-free method that only works in stationary scenes. 4dNDF [64] encodes the 4D scene into an implicit neural map, which can be used to distinguish the static map and dynamic objects. However, its application in real-time is limited. In addition, M-detector [54] proposes a network-free approach based on the occlusion principle. It requires manual tuning of numerous hyper-parameters when using different LiDARs or deploying in varying scenes. Moreover, to reduce the cost of manual labeling, several methods [10, 28] propose a pipeline that first generates coarse labels automatically and then refines them manually. In contrast to previous works on MOS, we employ self-supervised pre-training to enhance the few-shot MOS performance.

**3D Self-supervised Pre-training.** Effective self-supervised pre-training methods in NLP [5, 13, 40] and CV [18] have been extended to 3D data. Some methods [7, 15, 59] leverage BERT-like [13] or GPT-like [5, 40] pre-training on object CAD point clouds. Contrastive learning methods [8, 22, 27, 38, 42, 55] employ various transformations or augmentations to construct point/instance/scene-level contrastive loss, learning geometric or semantic information without manual labels. Additionally, Masked Auto-Encoder (MAE)-based methods [20, 26, 36, 39, 47, 56, 57, 63] extend MAE [18]

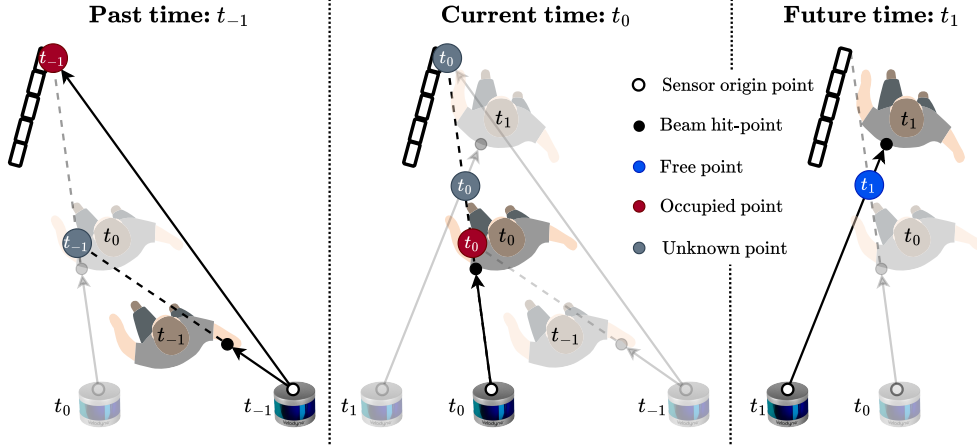


Figure 1. Illustration of temporal overlapping points in a realistic scenario. The color of points represents the occupancy state, and the index marked on the points indicates the observed time. For the two temporal overlapping points in the past and one in the future, their temporal occupancy states differ from the current occupancy states.

to 3D point clouds. These methods train an encoder by predicting a certain ratio of masked point cloud patches, which transfers well on object detection and semantic segmentation tasks. Subsequent works [21, 58, 65] apply NeRF-like [35] volumetric neural rendering to leverage multi-modal inputs and bridge the gap between 2D and 3D data. In summary, existing 3D self-supervised pre-training works lack temporal information and thus are unsuitable for MOS.

**LiDAR Observation Forecasting.** Existing works that involve temporal information of LiDAR data mainly focus on LiDAR observation forecasting, including point cloud and occupancy forecasting. Previous works on point cloud forecasting [32, 52, 53] directly predict the raw future LiDAR scans based on past ones. A recent study, 4Docc [23], claims the potential of forecasting as a scalable self-supervised task. Instead of directly predicting raw point clouds, 4Docc renders the future point clouds on a predicted occupancy map using known sensor intrinsics and extrinsics, enabling the network to focus on learning the world rather than sensor characteristics. Another generative approach, Copilot4D [60] introduces the concept of the world model. It tokenizes LiDAR scans and predicts future scans through discrete diffusion. However, the learned world knowledge is difficult to apply to downstream tasks due to the nature of heavy-decoder. ALSO [4] is a single-scan method that reconstructs the occupancy of a local surface and inspires UnO [1]. UnO is the most recent occupancy forecasting method that predicts the binary occupancy class of points sampled along future LiDAR rays. In this paper, we pre-train the backbone using the proposed **TOP** method instead of future observation forecasting.

### 3. Methodology

In this section, we introduce the self-supervised pre-training method **TOP**. Our method aims to pre-train an encoder for the downstream MOS task. The pre-training goal is to predict the occupancy states of temporal overlapping points and to reconstruct the current occupancy. We first introduce notations and problem formulation in Sec. 3.1. Then, we discuss the pre-processing of the temporal overlapping points in Sec. 3.2. Finally, we describe the pre-training objectives in Sec. 3.3.

#### 3.1. Problem Formulation

**Notations.** To begin with, we define a LiDAR scan as  $\mathbf{P} \in \mathbb{R}^{N \times 3}$ , where  $N$  is the number of points. We use subscript  $i$  to indicate the  $i^{th}$  point in  $\mathbf{P}$ , where each point  $\mathbf{p}_i \in \mathbb{R}^3$  ( $i = 1, 2, \dots, N$ ) contains  $xyz$  location.  $\mathbf{p}_i$  can be further described as a laser beam emitted from the sensor origin  $\mathbf{a} \in \mathbb{R}^3$  with its normalized beam direction  $\mathbf{d}_i \in \mathbb{R}^3$  and range  $r_i$ , leading to  $\mathbf{p}_i = \mathbf{a} + r_i \mathbf{d}_i$ . Although the laser beam is commonly modeled as an ideal ray, the real LiDAR beam exhibits a diverging radius as it travels, and this is referred to as beam divergence [31]. The beam divergence angle, denoted as  $\theta_{\text{dvg}}$ , is a constant for each type of LiDAR. When any part of the diverging beam hits an object, the LiDAR calculates the distance by time of flight and considers the beam center point as the hit-point, as shown in Fig. 3. To incorporate the temporal LiDAR sequence, we indicate scans at different timestamps with superscripts. For example, the scan at the current timestamp  $t_0$  is  $\mathbf{P}^{t_0} \in \mathbb{R}^{N \times 3}$ . For adjacent past/future timestamps  $\mathcal{T} = \{t_{-n} \dots t_{-1}, t_1 \dots t_n\}$ , we have  $\mathcal{P}_{\text{adj}} = \{\mathbf{P}^t \in \mathbb{R}^{N_i \times 3}\}_{t \in \mathcal{T}}$ . The  $j^{th}$  beam at time  $t$ , denoted as  $\mathbf{d}_j^t$ , can also be described by  $\mathbf{p}_j^t = \mathbf{a}^t + r_j^t \mathbf{d}_j^t$ .

**Point Clouds Encoding.** All scans in  $\mathcal{P}_{\text{adj}}$  are transformed

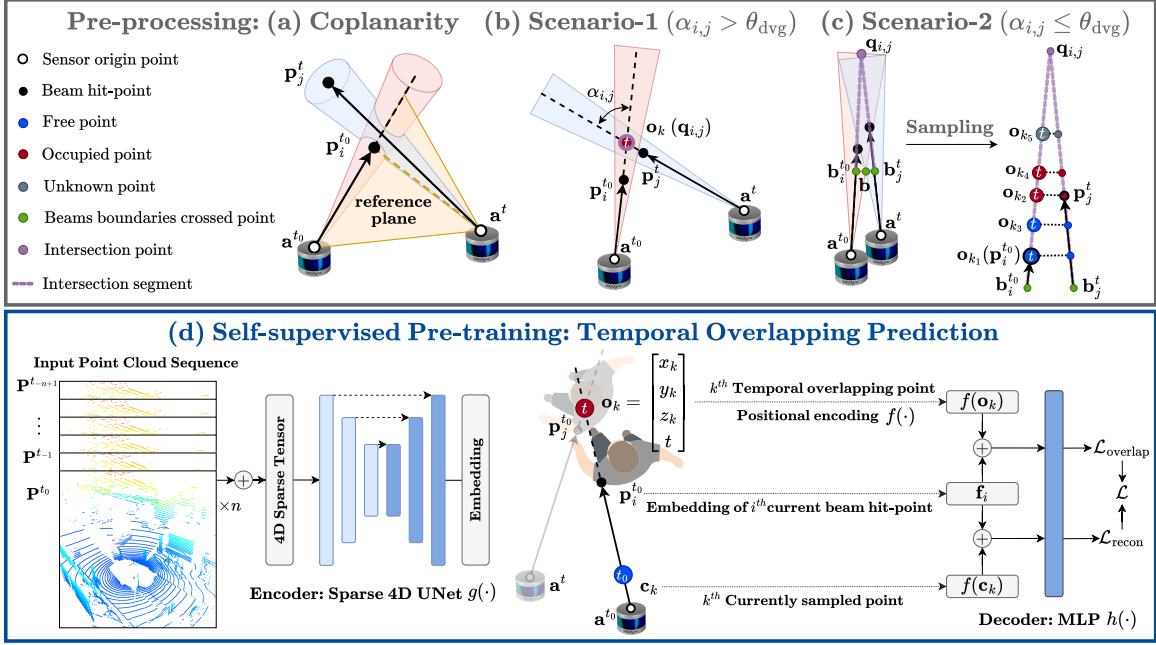


Figure 2. The overall pipeline. **Pre-processing:** (a) Coplanarity condition of two beams. (b) If the spatial angle between two beams  $\alpha_{i,j}$  exceeds the beam divergence angle  $\theta_{divg}$ , we sample the beams’ intersection point as the temporal overlapping point. The red and blue areas indicate beam divergence. (c) When  $\alpha_{i,j}$  is less than  $\theta_{divg}$ , the intersection segment is calculated to sample temporal overlapping points within it. **Pre-training:** (d) We use a sparse 4D UNet to embed the input scans. For the temporal overlapping prediction objective  $\mathcal{L}_{overlap}$ , the occupancy state of a temporal overlapping point is predicted based on its positional encoding and the embedding of the current beam hit-point. Similarly, the occupancy state of the currently sampled point is also predicted for the current reconstruction objective  $\mathcal{L}_{recon}$ .

to the local coordinate system of  $\mathbf{P}^{t_0}$  with the poses provided in the datasets. We take  $n$  current and past scans as network inputs  $\mathcal{P}_{in} = \{\mathbf{P}^{t-n+1} \dots \mathbf{P}^{t-1}, \mathbf{P}^{t_0}\}$ . Each point in  $\mathcal{P}_{in}$  is concatenated with its timestamp as a 4D point before being fed into the network. We apply a sparse 4D UNet encoder  $g(\cdot)$  used in [12, 33, 34, 50] to embed the spatiotemporal information of the 4D inputs:

$$\mathbf{F} = g(\mathcal{P}_{in}), \quad (1)$$

where  $\mathbf{F} \in \mathbb{R}^{N \times d}$  is the fully sparse features of the current scan  $\mathbf{P}^{t_0}$  with a feature dimension of  $d$ .

**Pre-training Loss.** We incorporate temporal overlapping points and their temporal occupancy states to pre-train the encoder  $g(\cdot)$ . As described in Fig. 1, temporal overlapping points are located on current LiDAR beams in  $\mathbf{P}^{t_0}$  and are also observed by adjacent past/future beams in  $\mathcal{P}_{adj}$ . Firstly, we denote the temporal overlapping points as  $\mathbf{O} \in \mathbb{R}^{M \times 4}$ , where  $M$  is the number of points and each point contains  $xyz$  position and the temporally observed timestamp  $t$ . Then, we use the LiDAR occupancy measurement model (introduced in Sec. 3.2) to describe the occupancy state labels of  $\mathbf{O}$ , denoted as  $\mathbf{S} \in \mathbb{R}^{M \times 3}$ . Each label is a three-dimensional one-hot vector indicating the occupancy

states “free”, “occupied”, and “unknown”. The overall pre-training goal consists of temporal occupancy prediction and current occupancy reconstruction, which is described as:

$$\mathcal{L} = \mathcal{L}_{overlap}(\mathbf{O}, \mathbf{S}, \mathbf{F}) + \mathcal{L}_{recon}(\mathbf{P}^{t_0}, \mathbf{F}). \quad (2)$$

### 3.2. Temporal Overlapping Pre-processing

As computing temporal overlapping during pre-training can be inefficient, we pre-process the LiDAR scans  $\mathbf{P}^{t_0}$  and  $\mathcal{P}_{adj}$  to produce temporal overlapping points  $\mathbf{O}$  and their occupancy states  $\mathbf{S}$ . We first identify coplanar beam pairs from  $\mathbf{P}^{t_0}$  and  $\mathcal{P}_{adj}$ , as coplanarity is a necessary condition for beams to have overlapping observations, as illustrated in Fig. 2(a). Then, we compute the intersection of coplanar beam pairs and sample temporal overlapping points. Depending on the spatial angle between two beams, we split the computation and sampling into two scenarios, shown in Fig. 2(b) and Fig. 2(c), respectively. We take an example beam pair for a clearer explanation: the  $i^{th}$  beam at time  $t_0$  and the  $j^{th}$  beam at time  $t$  ( $\mathbf{d}_i^{t_0}, \mathbf{d}_j^t$ ), emitted from ( $\mathbf{a}^{t_0}, \mathbf{a}^t$ ) and hitting ( $\mathbf{p}_i^{t_0}, \mathbf{p}_j^t$ ). When a beam pair ( $\mathbf{d}_i^{t_0}, \mathbf{d}_j^t$ ) generates the  $k^{th}$  temporal overlapping point  $\mathbf{o}_k$ , we record the  $(i, j, k)$  correspondence for subsequent usage in Sec. 3.3.



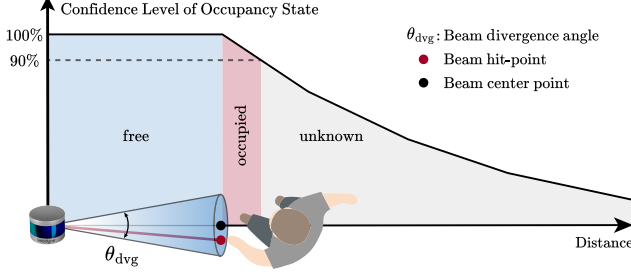


Figure 3. **LiDAR beam divergence model:** The bottom-left blue cone illustrates a real diverging beam, where the beam radius expands as the traversed distance increases. When any point within the beam spot hits an obstacle (indicated by the real hit-point colored in red), the center point of the beam spot (colored in black) is considered as the measured point. **LiDAR occupancy measurement model:** The occupancy state is confidently classified as free before reaching the beam hit-point. Then, the confidence level exponentially decays from the beam hit-point onward. A small area of high confidence after the beam hit-point is categorized as the occupied class, while the remaining areas are deemed unknown.

**Coplanarity.** We define a reference plane formed by  $(\mathbf{a}^{t_0}, \mathbf{a}^t, \mathbf{p}_i^{t_0})$ , illustrated as the yellow triangle in Fig. 2(a). The unit normal vector of this plane is:

$$\mathbf{n}_i^t = \mathbf{d}_i^{t_0} \times \frac{\mathbf{a}^t}{\|\mathbf{a}^t\|}. \quad (3)$$

The space angle between beam  $\mathbf{d}_j^t$  and the plane is:

$$\theta_{i,j} = \arccos(\mathbf{n}_i^t \cdot \mathbf{d}_j^t) - \frac{\pi}{2}. \quad (4)$$

Based on the physical beam divergence, if  $|\theta_{i,j}| \leq \frac{1}{2}\theta_{dvg}$ , we assume the two beams  $(\mathbf{d}_i^{t_0}, \mathbf{d}_j^t)$  are coplanar. All coplanar beam pairs are split into two scenarios based on the value of their spatial angle  $\alpha_{i,j} = \arccos(\mathbf{d}_i^{t_0} \cdot \mathbf{d}_j^t)$ .

**Scenario-1** ( $\alpha_{i,j} > \theta_{dvg}$ ). This scenario describes most overlapping cases where the spatial angle between two beams exceeds the beam divergence angle, as shown in Fig. 2(b). The beam intersection is small, thus being considered as a point  $\mathbf{q}_{i,j}$ , which is the intersection of the two beams' centerlines. The  $\mathbf{q}_{i,j}$  is solved from the parameter equations of the two beams:

$$\mathbf{q}_{i,j} = \frac{\mathbf{a}^t \times \mathbf{d}_j^t \cdot \mathbf{m}_{i,j}}{\mathbf{m}_{i,j} \cdot \mathbf{m}_{i,j}} \cdot \mathbf{d}_i^{t_0}, \quad (5)$$

where  $\mathbf{m}_{i,j} = \mathbf{d}_i^{t_0} \times \mathbf{d}_j^t$  is the unit common perpendicular line of the two beams. In this scenario, the intersection point  $\mathbf{q}_{i,j}$  is selected as the  $k^{th}$  temporal overlapping point  $\mathbf{o}_k$ .

**Scenario-2** ( $\alpha_{i,j} \leq \theta_{dvg}$ ). When the spatial angle between two beams is less than the beam divergence, the intersection of the two beams can no longer be considered as a point but

an area, as shown in Fig. 2(c). In this scenario, we compute the intersection segments (purple dashed lines) on the centerlines for subsequent sampling. Firstly, we obtain the end-point  $\mathbf{q}_{i,j}$  from the beam intersection similar to Scenario-1. Then, we approximate the starting point  $\mathbf{b}_i^{t_0}$  and  $\mathbf{b}_j^t$  as the projection from a point  $\mathbf{b}$  to the two beams. Here,  $\mathbf{b}$  is the crossed point of the boundaries of the two beams. Given that the spatial angle  $\alpha_{i,j}$  is small, we make two approximations to compute the starting points: (1) We approximate that the two intersection segments share the same length. (2) We approximate that the distance between the two starting points  $\mathbf{b}_i^{t_0}$  and  $\mathbf{b}_j^t$  is equal to the sum of the beam radius at the two points. The detailed formulas for computing  $\mathbf{b}_i^{t_0}$  and  $\mathbf{b}_j^t$  are in the appendix.

Since the overlap between two beams is an area, we sample 5 temporal overlapping points inside the intersection segment, as shown in Fig. 2(c) right:  $\mathbf{o}_{k_1}$ , the beam hit point  $\mathbf{p}_i^{t_0}$ ;  $\mathbf{o}_{k_2}$ , the projection of  $\mathbf{p}_j^t$  on  $\mathbf{d}_i^{t_0}$ ;  $\mathbf{o}_{k_3}$ , the center of  $(\mathbf{o}_{k_1}, \mathbf{o}_{k_2})$ ;  $\mathbf{o}_{k_4}$ , the center of  $(\mathbf{o}_{k_1}, \mathbf{q}_{i,j})$ ;  $\mathbf{o}_{k_5}$ , the center of  $(\mathbf{o}_{k_2}, \mathbf{q}_{i,j})$ . Their occupancy states at timestamp  $t$  are given by the states of their projection points on  $\mathbf{d}_j^t$ .

**LiDAR Occupancy Measurement Model.** The LiDAR occupancy measurement model [1, 43] partitions the space between the sensor origin to infinity along the beam direction into three areas with different occupancy states, as shown in Fig. 3. For the  $k^{th}$  temporal overlapping point  $\mathbf{o}_k$  generated from the overlap beams pair  $(\mathbf{d}_i^{t_0}, \mathbf{d}_j^t)$ , the confidence level  $w_{\text{conf}}$  of the measured occupancy state of  $\mathbf{o}_k$  is 100% when  $\mathbf{o}_k$  lies inside the physically traversed areas of the beam (blue area in Fig. 3). It then exponentially decays after the hit-point  $\mathbf{p}$ , as described below:

$$w_{\text{conf}}(\mathbf{o}_k, \mathbf{p}_j^t) = \begin{cases} 1, & \text{if } 0 \leq \|\mathbf{o}_k\| \leq \|\mathbf{p}_j^t\|, \\ e^{-(\|\mathbf{o}_k\| - \|\mathbf{p}_j^t\|)}, & \text{if } \|\mathbf{o}_k\| > \|\mathbf{p}_j^t\|. \end{cases} \quad (6)$$

The occupancy state of  $\mathbf{o}_k$  is denoted as  $\mathbf{s}_k$ , which is described as:

$$\mathbf{s}_k = \begin{cases} [1, 0, 0], & \text{if } 0 \leq \|\mathbf{o}_k\| < \|\mathbf{p}_j^t\|, \\ [0, 1, 0], & \text{if } \|\mathbf{o}_k\| = \|\mathbf{p}_j^t\| \text{ or } \lambda_{\text{occ}} \leq w_{\text{conf}}(\mathbf{o}_k, \mathbf{p}_j^t), \\ [0, 0, 1], & \text{if } w_{\text{conf}}(\mathbf{o}_k, \mathbf{p}_j^t) < \lambda_{\text{occ}}, \end{cases} \quad (7)$$

where  $\mathbf{s}_k$  is a one-hot vector indicating “free”, “occupied” and “unknown” occupancy states, and  $\lambda_{\text{occ}}$  is the confidence level threshold of the occupied state.

### 3.3. Training Objectives

For self-supervised pre-training, the primary objective is temporal overlapping prediction, which involves predicting  $\mathbf{s}_k$  from the  $i^{th}$  current point's feature  $\mathbf{f}_i$  and the positional information of  $\mathbf{o}_k$  using a shallow MLP decoder  $h(\cdot)$ :

$$\mathbf{u}_k = h(f(\mathbf{o}_k) + \mathbf{f}_i) \in \mathbb{R}^3, \quad (8)$$

where  $\mathbf{u}_k$  is the predicted probabilities of three occupancy states, and  $f(\mathbf{o}_k) \in \mathbb{R}^d$  denotes the sine-cosine 4D positional encoding vector as described in [49]. Temporal overlapping prediction is described as a Cross-Entropy loss:

$$\mathcal{L}_{\text{overlap}} = -\frac{1}{M} \sum_{k=1}^M w_{\text{conf}}(\mathbf{o}_k, \mathbf{p}_j^t) \cdot \mathbf{w}_s \cdot \mathbf{s}_k \cdot \log(\mathbf{u}_k), \quad (9)$$

where  $\mathbf{w}_s$  is a constant weight vector for each occupancy state, and the  $(i, j, k)$  correspondence is introduced in Sec. 3.2.

Additionally, we reconstruct the current occupancy using the input scans, which serves as a regularization term in the total loss. We randomly select  $M'$  occupied and free points on each current beam. For the  $k^{\text{th}}$  point  $\mathbf{c}_k$  sampled on the  $i^{\text{th}}$  current beam, it includes the spatial position and timestamp  $t_0$ . The ground truth occupancy label is  $\mathbf{s}_k$ , and the predicted probability is  $\mathbf{v}_k$ . The reconstruction objective is also specified as a Cross-Entropy loss:

$$\begin{aligned} \mathbf{v}_k &= h(f(\mathbf{c}_k) + \mathbf{f}_i) \in \mathbb{R}^3, \\ \mathcal{L}_{\text{recon}} &= -\frac{1}{NM'} \sum_{k=1}^{NM'} \mathbf{w}_s \cdot \mathbf{s}_k \cdot \log(\mathbf{v}_k). \end{aligned} \quad (10)$$

$$(11)$$

## 4. Evaluation Metrics

In this section, we propose a mean object-level metric denoted as  $\text{mIoU}_{\text{obj}}$  to tackle the biased weighting issue in the conventional IoU metric. Previous methods [9, 33, 34, 50] have relied solely on IoU as the evaluation metric. However, IoU implicitly gives larger weight to objects with more scanned points due to its point-wise nature. Objects of varying geometric sizes and distances to the LiDAR may result in different numbers of scanned points. Nevertheless, these objects are equally important in practical MOS applications and should not be weighted based on the number of scanned points. To further illustrate the impact of this bias on MOS performance evaluation, we conduct a statistical analysis: we sort all moving objects in the nuScenes train-val split based on the number of scanned points, and then calculate the cumulative distribution of moving objects and scanned points. The results indicate that the top 75.22% of objects with the fewest scanned points only contribute to 15.49% of the total points, while 90.06% of objects contribute to 37.02% of the points, revealing that a few objects with more points heavily influence the conventional IoU metric. The cumulative distribution is provided in the appendix.

The proposed metric  $\text{mIoU}_{\text{obj}}$  calculates the IoU for each moving object and computes the average, ensuring equal weighting for each moving object:

$$\text{mIoU}_{\text{obj}} = \frac{1}{m} \sum_{i=1}^m \frac{\text{TP}_i}{\text{TP}_i + \text{FP}_i}, \quad (12)$$

where  $m$  denotes the number of moving objects,  $\text{TP}_i$  and  $\text{FP}_i$  indicate the true positive and false positive classifications of the points belonging to  $i^{\text{th}}$  moving object. False negatives are not involved in the  $\text{mIoU}_{\text{obj}}$  as all points are classified as the moving (positive) class.

Additionally, in the nuScenes train-val split, ego vehicles' moving points account for 76.72% of all moving points, which can heavily influence the IoU. However, in autonomous driving scenarios, we already know the movement of the ego vehicle and do not need to predict it. Therefore, we utilize a refined IoU metric called  $\text{IoU}_{\text{w/o}}$ , calculated as described in [9, 33, 34] but excluding the scanned ego vehicle points.

For a more precise and robust evaluation of the MOS performance, we use both metrics:  $\text{mIoU}_{\text{obj}}$  assesses performance on all moving objects, while  $\text{IoU}_{\text{w/o}}$  reflects overall performance, incorporating false negatives.

## 5. Experiments

### 5.1. Experiments Setup

**Datasets.** We pretrain the encoder on the nuScenes dataset [6], which utilizes a 32-beam Velodyne LiDAR for data collection. The beam divergence angle  $\theta_{\text{div}}$  specified by the manufacturer is 0.003 rad. We perform few-shot experiments on the nuScenes dataset. Previous methods [34, 46] convert nuScenes object attributes into MOS labels. However, these attributes do not precisely describe the object's motion state. Moreover, some objects lack attributes and will be overlooked during training or evaluation. To overcome this limitation, we refine MOS labels by incorporating object attributes and speed. Speed is computed from object bounding boxes and is used to classify motion states by static and moving speed thresholds. We introduce a speed range between these thresholds to categorize objects with unclear motion states into an unknown class, such as cars that are just starting or hesitant pedestrians. More details are available in the appendix. We also conduct few-shot cross-dataset transfer experiments on the SemanticKITTI [3] MOS benchmark [9], which employs a 64-beam Velodyne LiDAR for data collection.

**Implementation Details.** In our setup, we have  $n = 6$ , where  $\mathcal{P}_{\text{adj}}$  includes 6 past scans and 6 future scans, and the input sequence  $\mathcal{P}_{\text{in}}$  comprises 6 scans. All scans are sampled at 2Hz. The confidence cutoff threshold for the occupied state is  $\lambda_{\text{occ}} = 0.9$ . We apply data augmentation techniques from [33, 37] and discard points outside a bounded area based on [1, 23]. Our encoder is the sparse 4D UNet backbone, commonly used in MOS methods [33, 34]. The quantization size for the sparse backbone is 0.1m, and the feature dimension  $d = 128$ . For the temporal overlapping prediction objective, all occupied class samples are included due to their scarcity, while 5 times the number of oc-

cupied samples are randomly selected for the free class and the same amount for the unknown class in each training iteration. As for the current occupancy reconstruction objective, we select 5 occupied points and 25 free points on each current beam ( $M' = 30$ ). The class weight is  $\mathbf{w}_s = [1, 5, 1]$  for free, occupied, and unknown class. We use a fixed random seed for all experiments to ensure reproducibility. Detailed optimizer settings are in the appendix.

**Baselines.** We use the SOTA supervised MOS method 4DMOS [33] as the training-from-scratch baseline. Additionally, we implement the SOTA LiDAR observation forecasting methods 4Docc [23] and UnO [1], along with the occupancy-based 3D method ALSO [4], as the self-supervised pre-training baselines. All baselines utilize the same sparse 4D UNet [12, 33] encoder with their respective original decoders.

## 5.2. Few-shot Results on nuScenes

We perform few-shot MOS experiments on the nuScenes dataset. All methods are first pre-trained on full sequences from the nuScenes train split. Then the pre-trained encoder of the last epoch is chosen and fine-tuned with labeled MOS data using binary Cross-Entropy loss. We randomly select 5%/10%/20%/50% of sequences from the nuScenes train split for MOS fine-tuning. To assess the convergence performance, all models are trained for a sufficient number of epochs until convergence. As it is not possible to assign weights to the two metrics to select a single “best” model, we can only choose two best models separately based on each metric. We present the test results on full sequences from the nuScenes val split in Tab. 1.

Our pre-training method improves training-from-scratch baseline across all fine-tuning data amounts. Our method achieves significant improvement in  $\text{mIoU}_{\text{obj}}$ , up to 12.17% relative improvement from 24.98% to 28.03%  $\text{mIoU}_{\text{obj}}$  when using 10% data, while the improvement in  $\text{IoU}_{\text{w/o}}$  is less pronounced. This is because we detect more moving objects with less number of points (such as pedestrians or cycles), which account for a small proportion of the total points. It is noteworthy that UnO also shows some increases on  $\text{mIoU}_{\text{obj}}$ , while the  $\text{IoU}_{\text{w/o}}$  all decreases. This result indicates that the performance of pre-training by UnO is not consistent, and it introduces more false negatives when detecting moving objects. This will lead to erroneous moving object alerts in MOS applications and cause incorrect path planning. In contrast, our method demonstrates consistent results in most cases. We visualize some results in Fig. 4.

## 5.3. Transferring Results on SemanticKITTI

To evaluate the transferability of the learned spatiotemporal representations, we fine-tune the pre-trained 4D UNet encoder on the SemanticKITTI dataset. We train the model on 10%/20%/50% random samples from SemanticKITTI train

Data	Pretrain	Best $\text{mIoU}_{\text{obj}}$		Best $\text{IoU}_{\text{w/o}}$	
		$\text{mIoU}_{\text{obj}}$	$\text{IoU}_{\text{w/o}}$	$\text{mIoU}_{\text{obj}}$	$\text{IoU}_{\text{w/o}}$
5%	No	24.27	34.96	23.20	35.05
	ALSO	18.68 <sup>-5.59</sup>	31.65 <sup>-3.31</sup>	17.57 <sup>-5.63</sup>	31.97 <sup>-3.07</sup>
	4Docc	22.14 <sup>-2.13</sup>	33.39 <sup>-1.57</sup>	21.02 <sup>-2.17</sup>	33.81 <sup>-1.24</sup>
	Uno	25.23 <sup>+0.96</sup>	34.31 <sup>-0.65</sup>	22.62 <sup>+0.58</sup>	34.90 <sup>-0.15</sup>
	<b>Ours</b>	<b>25.75<sup>+1.48</sup></b>	<b>35.94<sup>+0.98</sup></b>	<b>25.75<sup>+2.56</sup></b>	<b>35.94<sup>+0.90</sup></b>
10%	No	24.98	36.44	22.98	38.06
	ALSO	27.32 <sup>+2.34</sup>	35.74 <sup>-0.70</sup>	22.47 <sup>-0.51</sup>	<b>38.33<sup>+0.27</sup></b>
	4Docc	24.31 <sup>-0.67</sup>	36.01 <sup>-0.43</sup>	23.83 <sup>+0.86</sup>	37.46 <sup>-0.70</sup>
	Uno	26.38 <sup>+1.40</sup>	36.56 <sup>+0.12</sup>	22.00 <sup>-0.98</sup>	37.17 <sup>-0.89</sup>
	<b>Ours</b>	<b>28.03<sup>+3.04</sup></b>	<b>36.95<sup>+0.51</sup></b>	<b>24.69<sup>+1.72</sup></b>	38.06 <sup>+0.00</sup>
20%	No	25.59	44.25	24.52	<b>45.05</b>
	ALSO	26.68 <sup>+1.08</sup>	40.84 <sup>-3.41</sup>	25.81 <sup>+1.28</sup>	42.33 <sup>-2.72</sup>
	4Docc	26.01 <sup>+0.42</sup>	42.21 <sup>-2.04</sup>	24.58 <sup>+0.06</sup>	43.11 <sup>-1.94</sup>
	Uno	28.14 <sup>+2.55</sup>	43.63 <sup>-0.62</sup>	26.78 <sup>+2.26</sup>	43.97 <sup>-1.08</sup>
	<b>Ours</b>	<b>28.45<sup>+2.86</sup></b>	<b>44.30<sup>+0.05</sup></b>	<b>27.29<sup>+2.76</sup></b>	44.52 <sup>-0.53</sup>
50%	No	29.80	49.29	29.80	49.29
	ALSO	30.72 <sup>+0.91</sup>	47.34 <sup>-1.95</sup>	28.06 <sup>-1.75</sup>	48.10 <sup>-1.19</sup>
	4Docc	29.20 <sup>-0.60</sup>	46.73 <sup>-2.56</sup>	28.19 <sup>-1.62</sup>	48.19 <sup>-1.10</sup>
	Uno	29.54 <sup>-0.26</sup>	48.59 <sup>-0.70</sup>	28.81 <sup>-1.00</sup>	48.76 <sup>-0.53</sup>
	<b>Ours</b>	<b>30.58<sup>+0.78</sup></b>	<b>49.80<sup>+0.51</sup></b>	<b>30.58<sup>+0.78</sup></b>	<b>49.80<sup>+0.51</sup></b>

Table 1. Few-shot MOS results on the nuScenes dataset. The best performance in each column is in bold. The metric used for model selection is in bold in the table header.

set for enough epochs until convergence. As demonstrated in Tab. 2, **TOP** shows the best transferability on different LiDAR setups among all baselines. Fig. 5 displays the results on the SemanticKITTI dataset.

Data	Pretrain	Best $\text{mIoU}_{\text{obj}}$		Best $\text{IoU}_{\text{w/o}}$	
		$\text{mIoU}_{\text{obj}}$	$\text{IoU}_{\text{w/o}}$	$\text{mIoU}_{\text{obj}}$	$\text{IoU}_{\text{w/o}}$
10%	No	37.22	41.22	33.97	42.81
	ALSO	9.21 <sup>-28.01</sup>	7.33 <sup>-33.88</sup>	9.21 <sup>-24.77</sup>	7.76 <sup>-35.05</sup>
	4Docc	8.54 <sup>-28.68</sup>	13.35 <sup>-27.87</sup>	8.15 <sup>-25.82</sup>	13.45 <sup>-29.36</sup>
	Uno	36.66 <sup>-0.57</sup>	35.03 <sup>-6.19</sup>	27.83 <sup>-6.15</sup>	37.41 <sup>-5.41</sup>
	<b>Ours</b>	<b>44.68<sup>+7.46</sup></b>	<b>43.29<sup>+2.07</sup></b>	<b>43.36<sup>+9.39</sup></b>	<b>49.37<sup>+6.55</sup></b>
20%	No	47.41	47.38	45.39	48.77
	ALSO	23.37 <sup>-24.04</sup>	23.02 <sup>-24.36</sup>	23.37 <sup>-22.02</sup>	23.02 <sup>-25.75</sup>
	4Docc	25.61 <sup>-21.80</sup>	35.83 <sup>-11.55</sup>	25.23 <sup>-20.16</sup>	36.24 <sup>-12.53</sup>
	Uno	45.48 <sup>-1.92</sup>	42.09 <sup>-5.29</sup>	43.77 <sup>-1.62</sup>	46.09 <sup>-2.68</sup>
	<b>Ours</b>	<b>58.45<sup>+11.04</sup></b>	<b>50.21<sup>+2.82</sup></b>	<b>58.45<sup>+13.06</sup></b>	<b>50.21<sup>+1.44</sup></b>
50%	No	53.13	56.35	48.20	59.20
	ALSO	49.82 <sup>-3.32</sup>	57.07 <sup>+0.72</sup>	44.27 <sup>-3.93</sup>	60.25 <sup>+1.04</sup>
	4Docc	39.23 <sup>-13.91</sup>	44.48 <sup>-11.88</sup>	38.36 <sup>-9.84</sup>	44.87 <sup>-14.33</sup>
	Uno	53.61 <sup>+0.48</sup>	54.97 <sup>-1.38</sup>	<b>52.73<sup>+4.53</sup></b>	57.06 <sup>-2.14</sup>
	<b>Ours</b>	<b>55.81<sup>+2.67</sup></b>	<b>58.85<sup>+2.50</sup></b>	52.11 <sup>+3.91</sup>	<b>61.55<sup>+2.35</sup></b>

Table 2. Cross-dataset transferring results on the SemanticKITTI MOS benchmark. The best performance in each column is in bold. The metric used for model selection is in bold in the table header.

## 5.4. Semantic Segmentation Results on nuScenes

We also assess how well our pre-training generalizes to a new downstream task by conducting a few-shot semantic segmentation experiment on the nuScenes dataset. We fine-tune the pre-trained encoders for a sufficient number of epochs using 10% of the train split sequences. As shown in Tab. 3, **TOP** shows a +0.42% mIoU improvement compared to the training-from-scratch baseline, while the performance of other methods notably declines. We suspect that the performance drop of 4Docc and UnO may be due to the complex “flow” information causing network overfitting, as discussed in Sec. 1. This experiment demonstrates the potential generalization capability of **TOP** pre-training across different downstream tasks.

Pretrain	No	ALSO	4Docc	UnO	Ours
mIoU	50.55	50.26 <sup>-0.29</sup>	47.49 <sup>-3.06</sup>	48.06 <sup>-2.49</sup>	<b>50.97<sup>+0.42</sup></b>

Table 3. Few-shot results on nuScenes semantic segmentation.

## 5.5. Ablation Study on Training Objectives

We perform an ablation study on the two training objectives  $\mathcal{L}_{\text{overlap}}$  and  $\mathcal{L}_{\text{recon}}$ . Results in Tab. 4 indicate that employing both objectives enhances overall performance compared to using only the temporal overlapping prediction objective. As current occupancy reconstruction is straightforward and its loss converges rapidly, we speculate it acts as a regularization term to prevent overfitting.

Objectives	Best mIoU <sub>obj</sub>		Best IoU <sub>w/o</sub>	
	mIoU <sub>obj</sub>	IoU <sub>w/o</sub>	mIoU <sub>obj</sub>	IoU <sub>w/o</sub>
$\mathcal{L}_{\text{overlap}}$	24.559	34.785	22.639	35.350
$\mathcal{L}_{\text{overlap}} + \mathcal{L}_{\text{recon}}$	<b>25.75</b>	<b>35.94</b>	<b>25.75</b>	<b>35.94</b>

Table 4. Ablation study on two training objectives.

## 6. Conclusion

In this paper, we propose a self-supervised pre-training method called **Temporal Overlapping Prediction (TOP)** for moving object segmentation (MOS). **TOP** predicts the occupancy states of temporal overlapping points to help the model learn spatiotemporal representations for MOS. We evaluate the effectiveness of **TOP** through few-shot experiments on nuScenes and cross-dataset transfer experiments on SemanticKITTI. **TOP** consistently improves both the object-level metric and the point-level metric, demonstrating strong transferability across LiDAR setups. Additionally, the improved performance in semantic segmentation suggests potential generalization to more downstream tasks. Further investigation of the effectiveness of **TOP** in other temporal tasks such as object tracking is worthwhile.

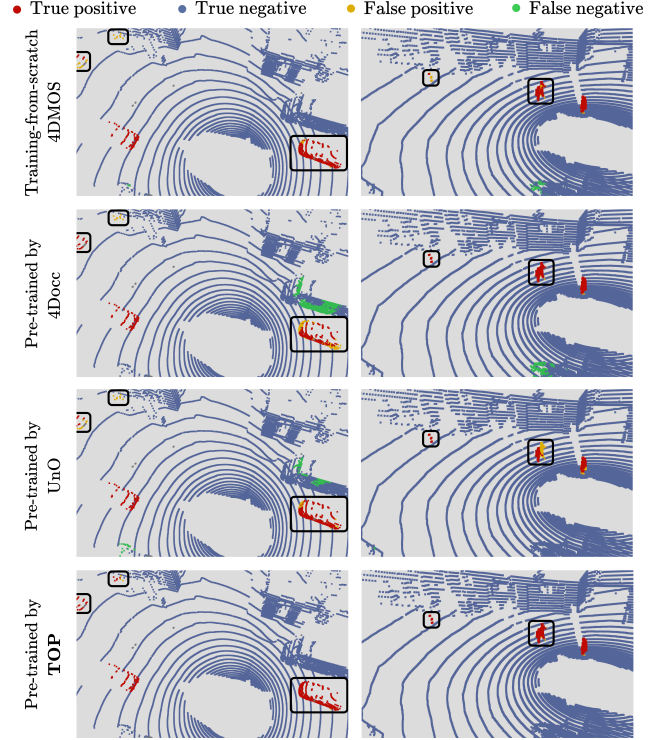


Figure 4. Visualization of the nuScenes MOS results.

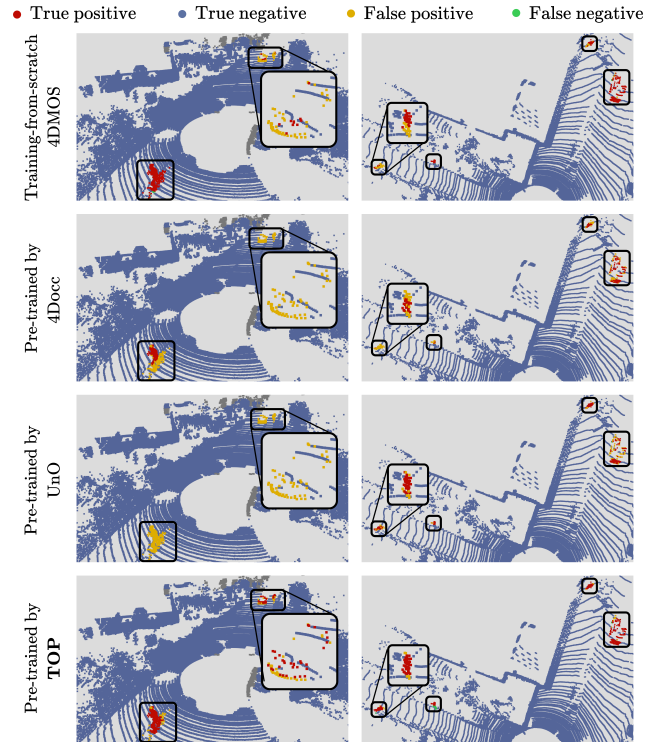


Figure 5. Visualization of the SemanticKITTI MOS results.



## References

- [1] Ben Agro, Quinlan Sykora, Sergio Casas, Thomas Gilles, and Raquel Urtasun. Uno: Unsupervised occupancy fields for perception and forecasting. In *Proceedings of the IEEE/CVF Conference on Computer Vision and Pattern Recognition*, pages 14487–14496, 2024. 1, 2, 3, 5, 6, 7
- [2] Stefan Andreas Baur, David Josef Emmerichs, Frank Moosmann, Peter Pinggera, Björn Ommer, and Andreas Geiger. Slim: Self-supervised lidar scene flow and motion segmentation. In *Proceedings of the IEEE/CVF International Conference on Computer Vision*, pages 13126–13136, 2021. 2
- [3] J. Behley, M. Garbade, A. Milioto, J. Quenzel, S. Behnke, C. Stachniss, and J. Gall. SemanticKITTI: A Dataset for Semantic Scene Understanding of LiDAR Sequences. In *Proc. of the IEEE/CVF International Conf. on Computer Vision (ICCV)*, 2019. 1, 2, 6
- [4] Alexandre Boulch, Corentin Sautier, Björn Michele, Gilles Puy, and Renaud Marlet. ALSO: Automotive lidar self-supervision by occupancy estimation. In *International Conference on Computer Vision and Pattern Recognition (CVPR)*, 2023. 2, 3, 7
- [5] Tom B Brown. Language models are few-shot learners. *arXiv preprint arXiv:2005.14165*, 2020. 1, 2
- [6] Holger Caesar, Varun Bankiti, Alex H. Lang, Sourabh Vora, Venice Erin Liong, Qiang Xu, Anush Krishnan, Yu Pan, Giancarlo Baldan, and Oscar Beijbom. nuscenes: A multimodal dataset for autonomous driving. *arXiv preprint arXiv:1903.11027*, 2019. 1, 2, 6
- [7] Guangyan Chen, Meiling Wang, Yi Yang, Kai Yu, Li Yuan, and Yufeng Yue. Pointgpt: Auto-regressively generative pre-training from point clouds. *Advances in Neural Information Processing Systems*, 36, 2024. 2
- [8] Runjian Chen, Yao Mu, Runsen Xu, Wenqi Shao, Chenhan Jiang, Hang Xu, Zhenguo Li, and Ping Luo. Co<sup>3</sup>: Cooperative unsupervised 3d representation learning for autonomous driving. *arXiv preprint arXiv:2206.04028*, 2022. 2
- [9] Xieyuanli Chen, Shijie Li, Benedikt Mersch, Louis Wiesmann, Jürgen Gall, Jens Behley, and Cyrill Stachniss. Moving object segmentation in 3d lidar data: A learning-based approach exploiting sequential data. *IEEE Robotics and Automation Letters*, 6(4):6529–6536, 2021. 1, 2, 6
- [10] Xieyuanli Chen, Benedikt Mersch, Lucas Nunes, Rodrigo Marcuzzi, Ignacio Vizzo, Jens Behley, and Cyrill Stachniss. Automatic labeling to generate training data for online lidar-based moving object segmentation. *IEEE Robotics and Automation Letters*, 7(3):6107–6114, 2022. 2
- [11] Jintao Cheng, Kang Zeng, Zhuoxu Huang, Xiaoyu Tang, Jin Wu, Chengxi Zhang, Xieyuanli Chen, and Rui Fan. Mf-mos: A motion-focused model for moving object segmentation. *arXiv preprint arXiv:2401.17023*, 2024. 2
- [12] Christopher Choy, JunYoung Gwak, and Silvio Savarese. 4d spatio-temporal convnets: Minkowski convolutional neural networks. In *Proceedings of the IEEE Conference on Computer Vision and Pattern Recognition*, pages 3075–3084, 2019. 2, 4, 7
- [13] Jacob Devlin. Bert: Pre-training of deep bidirectional transformers for language understanding. *arXiv preprint arXiv:1810.04805*, 2018. 1, 2
- [14] Alexey Dosovitskiy. An image is worth 16x16 words: Transformers for image recognition at scale. *arXiv preprint arXiv:2010.11929*, 2020. 1
- [15] Kexue Fu, Peng Gao, ShaoLei Liu, Linhao Qu, Longxiang Gao, and Manning Wang. Pos-bert: Point cloud one-stage bert pre-training. *Expert Systems with Applications*, 240: 122563, 2024. 2
- [16] Zan Gojcic, Or Litany, Andreas Wieser, Leonidas J Guibas, and Tolga Birdal. Weakly supervised learning of rigid 3d scene flow. In *Proceedings of the IEEE/CVF conference on computer vision and pattern recognition*, pages 5692–5703, 2021. 2
- [17] Kaiming He, Haoqi Fan, Yuxin Wu, Saining Xie, and Ross Girshick. Momentum contrast for unsupervised visual representation learning. In *Proceedings of the IEEE/CVF conference on computer vision and pattern recognition*, pages 9729–9738, 2020. 1
- [18] Kaiming He, Xinlei Chen, Saining Xie, Yanghao Li, Piotr Dollár, and Ross Girshick. Masked autoencoders are scalable vision learners. In *Proceedings of the IEEE/CVF conference on computer vision and pattern recognition*, pages 16000–16009, 2022. 1, 2
- [19] Pengcheng He, Xiaodong Liu, Jianfeng Gao, and Weizhu Chen. Deberta: Decoding-enhanced bert with disentangled attention. *arXiv preprint arXiv:2006.03654*, 2020. 1
- [20] Georg Hess, Johan Jaxing, Elias Svensson, David Hagerman, Christoffer Petersson, and Lennart Svensson. Masked autoencoder for self-supervised pre-training on lidar point clouds. In *Proceedings of the IEEE/CVF winter conference on applications of computer vision*, pages 350–359, 2023. 2
- [21] Di Huang, Sida Peng, Tong He, Honghui Yang, Xiaowei Zhou, and Wanli Ouyang. Ponder: Point cloud pre-training via neural rendering. In *Proceedings of the IEEE/CVF International Conference on Computer Vision*, pages 16089–16098, 2023. 3
- [22] Siyuan Huang, Yichen Xie, Song-Chun Zhu, and Yixin Zhu. Spatio-temporal self-supervised representation learning for 3d point clouds. In *Proceedings of the IEEE/CVF International Conference on Computer Vision*, pages 6535–6545, 2021. 2
- [23] Tarasha Khurana, Peiyun Hu, David Held, and Deva Ramanan. Point cloud forecasting as a proxy for 4d occupancy forecasting. In *Proceedings of the IEEE/CVF Conference on Computer Vision and Pattern Recognition*, pages 1116–1124, 2023. 1, 2, 3, 6, 7
- [24] Jaeyeul Kim, Jungwan Woo, and Sunghoon Im. Rvmos: Range-view moving object segmentation leveraged by semantic and motion features. *IEEE Robotics and Automation Letters*, 7(3):8044–8051, 2022. 2
- [25] Thomas Kreutz, Max Mühlhäuser, and Alejandro Sanchez Guinea. Unsupervised 4d lidar moving object segmentation in stationary settings with multivariate occupancy time series. In *Proceedings of the IEEE/CVF Winter Conference on Applications of Computer Vision*, pages 1644–1653, 2023. 2
- [26] Georg Kispel, David Schinagl, Christian Fruhwirth-Reisinger, Horst Possegger, and Horst Bischof. Maeli:

- Masked autoencoder for large-scale lidar point clouds. In *Proceedings of the IEEE/CVF Winter Conference on Applications of Computer Vision*, pages 3383–3392, 2024. 2
- [27] Hanxue Liang, Chenhan Jiang, Dapeng Feng, Xin Chen, Hang Xu, Xiaodan Liang, Wei Zhang, Zhenguo Li, and Luc Van Gool. Exploring geometry-aware contrast and clustering harmonization for self-supervised 3d object detection. In *Proceedings of the IEEE/CVF International Conference on Computer Vision*, pages 3293–3302, 2021. 2
- [28] Hyungtae Lim, Seoyeon Jang, Benedikt Mersch, Jens Behley, Hyun Myung, and Cyrill Stachniss. Helimos: A dataset for moving object segmentation in 3d point clouds from heterogeneous lidar sensors. *arXiv preprint arXiv:2408.06328*, 2024. 2
- [29] Yancong Lin and Holger Caesar. Icp-flow: Lidar scene flow estimation with icp. In *Proceedings of the IEEE/CVF Conference on Computer Vision and Pattern Recognition*, pages 15501–15511, 2024. 2
- [30] Yinhan Liu. Roberta: A robustly optimized bert pretraining approach. *arXiv preprint arXiv:1907.11692*, 364, 2019. 1
- [31] Yunfei Long and Daniel Morris. Lidar essential beam model for accurate width estimation of thin poles. In *2020 IEEE/RSJ International Conference on Intelligent Robots and Systems (IROS)*, pages 2281–2287. IEEE, 2020. 2, 3
- [32] Benedikt Mersch, Xieyuanli Chen, Jens Behley, and Cyrill Stachniss. Self-supervised point cloud prediction using 3d spatio-temporal convolutional networks. In *Conference on Robot Learning*, pages 1444–1454. PMLR, 2022. 1, 3
- [33] Benedikt Mersch, Xieyuanli Chen, Ignacio Vizzo, Lucas Nunes, Jens Behley, and Cyrill Stachniss. Receding moving object segmentation in 3d lidar data using sparse 4d convolutions. *IEEE Robotics and Automation Letters*, 7(3):7503–7510, 2022. 1, 2, 4, 6, 7
- [34] Benedikt Mersch, Tiziano Guadagnino, Xieyuanli Chen, Ignacio Vizzo, Jens Behley, and Cyrill Stachniss. Building volumetric beliefs for dynamic environments exploiting map-based moving object segmentation. *IEEE Robotics and Automation Letters*, 2023. 1, 2, 4, 6
- [35] Ben Mildenhall, Pratul P Srinivasan, Matthew Tancik, Jonathan T Barron, Ravi Ramamoorthi, and Ren Ng. Nerf: Representing scenes as neural radiance fields for view synthesis. *Communications of the ACM*, 65(1):99–106, 2021. 3
- [36] Chen Min, Liang Xiao, Dawei Zhao, Yiming Nie, and Bin Dai. Occupancy-mae: Self-supervised pre-training large-scale lidar point clouds with masked occupancy autoencoders. *IEEE Transactions on Intelligent Vehicles*, 2023. 2
- [37] Lucas Nunes, Rodrigo Marcuzzi, Xieyuanli Chen, Jens Behley, and Cyrill Stachniss. Segcontrast: 3d point cloud feature representation learning through self-supervised segment discrimination. *IEEE Robotics and Automation Letters*, 7(2):2116–2123, 2022. 6
- [38] Lucas Nunes, Louis Wiesmann, Rodrigo Marcuzzi, Xieyuanli Chen, Jens Behley, and Cyrill Stachniss. Temporal Consistent 3D LiDAR Representation Learning for Semantic Perception in Autonomous Driving. In *Proc. of the IEEE/CVF Conf. on Computer Vision and Pattern Recognition (CVPR)*, 2023. 2
- [39] Yatian Pang, Wenxiao Wang, Francis EH Tay, Wei Liu, Yonghong Tian, and Li Yuan. Masked autoencoders for point cloud self-supervised learning. In *European conference on computer vision*, pages 604–621. Springer, 2022. 1, 2
- [40] Alec Radford. Improving language understanding by generative pre-training. 2018. 1, 2
- [41] Alec Radford, Jong Wook Kim, Chris Hallacy, Aditya Ramesh, Gabriel Goh, Sandhini Agarwal, Girish Sastry, Amanda Askell, Pamela Mishkin, Jack Clark, et al. Learning transferable visual models from natural language supervision. In *International conference on machine learning*, pages 8748–8763. PMLR, 2021. 1
- [42] Corentin Sautier, Gilles Puy, Alexandre Boulch, Renaud Marlet, and Vincent Lepetit. Bevcontrast: Self-supervision in bev space for automotive lidar point clouds. In *2024 International Conference on 3D Vision (3DV)*, pages 559–568. IEEE, 2024. 2
- [43] Alexander Schaefer, Lukas Luft, and Wolfram Burgard. An analytical lidar sensor model based on ray path information. *IEEE Robotics and Automation Letters*, 2(3):1405–1412, 2017. 5
- [44] Tao Song, Yunhao Liu, Ziyang Yao, and Xinkai Wu. Ssf-mos: Semantic scene flow assisted moving object segmentation for autonomous vehicles. *IEEE Transactions on Instrumentation and Measurement*, 2024. 2
- [45] Jiadai Sun, Yuchao Dai, Xianjing Zhang, Jintao Xu, Rui Ai, Weihao Gu, and Xieyuanli Chen. Efficient spatial-temporal information fusion for lidar-based 3d moving object segmentation. In *2022 IEEE/RSJ International Conference on Intelligent Robots and Systems (IROS)*, pages 11456–11463. IEEE, 2022. 2
- [46] Yuxiang Sun, Weixun Zuo, Huaiyang Huang, Peide Cai, and Ming Liu. Pointmoseg: Sparse tensor-based end-to-end moving-obstacle segmentation in 3-d lidar point clouds for autonomous driving. *IEEE Robotics and Automation Letters*, 6(2):510–517, 2020. 2, 6
- [47] Xiaoyu Tian, Haoxi Ran, Yue Wang, and Hang Zhao. Geomae: Masked geometric target prediction for self-supervised point cloud pre-training. In *Proceedings of the IEEE/CVF Conference on Computer Vision and Pattern Recognition*, pages 13570–13580, 2023. 2
- [48] Ivan Tishchenko, Sandro Lombardi, Martin R Oswald, and Marc Pollefeys. Self-supervised learning of non-rigid residual flow and ego-motion. In *2020 international conference on 3D vision (3DV)*, pages 150–159. IEEE, 2020. 2
- [49] A Vaswani. Attention is all you need. *Advances in Neural Information Processing Systems*, 2017. 6
- [50] Neng Wang, Chenghao Shi, Ruibin Guo, Huimin Lu, Zhiqiang Zheng, and Xieyuanli Chen. Insomos: Instance-aware moving object segmentation in lidar data. In *2023 IEEE/RSJ International Conference on Intelligent Robots and Systems (IROS)*, pages 7598–7605. IEEE, 2023. 1, 2, 4, 6
- [51] Xiaolong Wang and Abhinav Gupta. Unsupervised learning of visual representations using videos. In *Proceedings of the IEEE international conference on computer vision*, pages 2794–2802, 2015. 1

- [52] Xinshuo Weng, Jianren Wang, Sergey Levine, Kris Kitani, and Nicholas Rhinehart. Inverting the pose forecasting pipeline with spf2: Sequential pointcloud forecasting for sequential pose forecasting. In *Conference on robot learning*, pages 11–20. PMLR, 2021. [1](#), [3](#)
- [53] Xinshuo Weng, Junyu Nan, Kuan-Hui Lee, Rowan McAllister, Adrien Gaidon, Nicholas Rhinehart, and Kris M Kitani. S2net: Stochastic sequential pointcloud forecasting. In *European Conference on Computer Vision*, pages 549–564. Springer, 2022. [1](#), [3](#)
- [54] Huajie Wu, Yihang Li, Wei Xu, Fanze Kong, and Fu Zhang. Moving event detection from lidar point streams. *nature communications*, 15(1):345, 2024. [1](#), [2](#)
- [55] Saining Xie, Jiatao Gu, Demi Guo, Charles R Qi, Leonidas Guibas, and Or Litany. Pointcontrast: Unsupervised pre-training for 3d point cloud understanding. In *Computer Vision–ECCV 2020: 16th European Conference, Glasgow, UK, August 23–28, 2020, Proceedings, Part III 16*, pages 574–591. Springer, 2020. [1](#), [2](#)
- [56] Runsen Xu, Tai Wang, Wenwei Zhang, Runjian Chen, Jinkun Cao, Jiangmiao Pang, and Dahua Lin. Mv-jar: Masked voxel jigsaw and reconstruction for lidar-based self-supervised pre-training. In *Proceedings of the IEEE/CVF Conference on Computer Vision and Pattern Recognition*, pages 13445–13454, 2023. [2](#)
- [57] Honghui Yang, Tong He, Jiaheng Liu, Hua Chen, Boxi Wu, Binbin Lin, Xiaofei He, and Wanli Ouyang. Gd-mae: generative decoder for mae pre-training on lidar point clouds. In *Proceedings of the IEEE/CVF Conference on Computer Vision and Pattern Recognition*, pages 9403–9414, 2023. [2](#)
- [58] Honghui Yang, Sha Zhang, Di Huang, Xiaoyang Wu, Haoyi Zhu, Tong He, Shixiang Tang, Hengshuang Zhao, Qibo Qiu, Binbin Lin, et al. Unipad: A universal pre-training paradigm for autonomous driving. In *Proceedings of the IEEE/CVF Conference on Computer Vision and Pattern Recognition*, pages 15238–15250, 2024. [1](#), [3](#)
- [59] Xumin Yu, Lulu Tang, Yongming Rao, Tiejun Huang, Jie Zhou, and Jiwen Lu. Point-bert: Pre-training 3d point cloud transformers with masked point modeling. In *Proceedings of the IEEE/CVF conference on computer vision and pattern recognition*, pages 19313–19322, 2022. [1](#), [2](#)
- [60] Lunjun Zhang, Yuwen Xiong, Ze Yang, Sergio Casas, Rui Hu, and Raquel Urtasun. Learning unsupervised world models for autonomous driving via discrete diffusion. *arXiv preprint arXiv:2311.01017*, 2023. [1](#), [2](#), [3](#)
- [61] Qingwen Zhang, Yi Yang, Heng Fang, Ruoyu Geng, and Patric Jensfelt. DeFlow: Decoder of scene flow network in autonomous driving. In *2024 IEEE International Conference on Robotics and Automation (ICRA)*, pages 2105–2111, 2024. [2](#)
- [62] Qingwen Zhang, Yi Yang, Peizheng Li, Olov Andersson, and Patric Jensfelt. SeFlow: A self-supervised scene flow method in autonomous driving. In *European Conference on Computer Vision (ECCV)*, page 353–369. Springer, 2024. [2](#)
- [63] Renrui Zhang, Ziyu Guo, Peng Gao, Rongyao Fang, Bin Zhao, Dong Wang, Yu Qiao, and Hongsheng Li. Point-m2ae: multi-scale masked autoencoders for hierarchical point cloud pre-training. *Advances in neural information processing systems*, 35:27061–27074, 2022. [2](#)
- [64] Xingguang Zhong, Yue Pan, Cyrill Stachniss, and Jens Behley. 3d lidar mapping in dynamic environments using a 4d implicit neural representation. In *Proceedings of the IEEE/CVF Conference on Computer Vision and Pattern Recognition*, pages 15417–15427, 2024. [2](#)
- [65] Haoyi Zhu, Honghui Yang, Xiaoyang Wu, Di Huang, Sha Zhang, Xianglong He, Tong He, Hengshuang Zhao, Chunhua Shen, Yu Qiao, et al. Ponderv2: Pave the way for 3d foundation model with a universal pre-training paradigm. *arXiv preprint arXiv:2310.08586*, 2023. [3](#)